MSDE

ROYAL SOCIETY OF CHEMISTRY

PAPER

Cite this: *Mol. Syst. Des. Eng.*, 2022, 7, 1736

Developing Pd(II) based amphiphilic polymeric nanoparticles for pro-drug activation in complex media†

Anjana Sathyan, [a] Stephen Croke,[b] Ana M. Pérez-López,‡[b] Bas F. M. de Waal,[a] Asier Unciti-Broceta [b] and Anja R. A. Palmans *[a]

Novel approaches to targeted cancer therapy that combine improved efficacy of current chemotherapies while minimising side effects are highly sought after. The development of single-chain polymeric nanoparticles (SCPNs) as bio-orthogonal catalysts for targeted site-specific pro-drug activation is a promising avenue to achieve this. Currently, the application of SCPNs as bio-orthogonal catalysts is in its early stages due to reduced performance when increasing the medium's complexity. Herein, we present a systematic approach to identify the various aspects of SCPN-based catalytic systems, to improve their efficiency in future *in vitro*/*in vivo* studies. We developed amphiphilic polymers with a polyacrylamide backbone and functionalised with the Pd(II)-binding ligands triphenylphosphine and bipyridine. The resulting polymers collapse into small-sized nanoparticles (5–6 nm) with an inner hydrophobic domain that comprises the Pd(II) catalyst. We systematically evaluated the effect of polymer microstructure, ligand–metal complex, and substrate hydrophobicity on the catalytic activity of the nanoparticles for depropargylation reactions in water, PBS or DMEM. The results show that the catalytic activity of nanoparticles is primarily impacted by the ligand–metal complex while polymer microstructure has a minor influence. Moreover, the rate of reaction is increased for hydrophobic substrates. In addition, Pd(II) leaching studies confirmed little to no loss of Pd(II) from the hydrophobic interior which can reduce off-target toxicities in future applications. Careful deconstruction of the catalytic system revealed that covalent attachment of the ligand to the polymer backbone is necessary to retain its catalytic activity in cell culture medium while not in water. Finally, we activated anti-cancer pro-drugs based on 5-FU, paclitaxel, and doxorubicin using the best-performing catalytic SCPNs. We found that the rate of pro-drug activation in water was accelerated efficiently by catalytic SCPNs, whereas in cell culture medium the results depended on the type of protecting group and hydrophobicity of the prodrug. We believe our findings will aid in the development of suitable catalytic systems and pro-drugs for future *in vivo* applications.

Received 12th August 2022,
Accepted 14th September 2022

DOI: 10.1039/d2me00173j

rsc.li/molecular-engineering

Design, System, Application

Transition-metal-mediated bio-orthogonal reactions for synthesising drugs *in situ* that target tumour cells can help to develop side-effect-free cancer therapies. Challenges arise from insolubility of efficient catalysts or prodrugs in water, catalyst deactivation or sequestration by proteins in cells, biocompatibility, and the need for high activity at low substrate concentrations. Our approach to tackling these involves designing a catalytic system where the catalyst ligand is covalently attached to an amphiphilic polymer that folds around the metal–ligand complex into polymeric nanoparticles. The hydrophobic domain inside these polymeric nanoparticles ensures catalyst and substrate solubilisation and accumulation, resulting in high local concentrations and fast reactions. We report here on amphiphilic polymer-based designs with different ligands that bind to Pd(II) and tested the activation of propargyl-protected pro-dyes and pro-drugs in aqueous media of increasing complexity. We developed a systematic approach to determine factors that affect the performance of catalytic nanoparticles such as substrate hydrophobicity, nature of ligands, and microstructure of the polymers, which helped to find the best catalytic system based on stability, activity, and accessibility depending on the medium. The ability of our designed system to activate the several prodrugs motivates further improvements and development of catalytic nanoparticles for application in cancer therapies.

[a] *Laboratory of Macromolecular and Organic Chemistry, Eindhoven University of Technology, P.O box 513, 5600 MB Eindhoven, The Netherlands.*
E-mail: a.palmans@tue.nl
[b] *Edinburgh Cancer Research, Institute of Genetics and Cancer, University of Edinburgh, Crewe Road South, Edinburgh, EH4 2XR, UK*

† Electronic supplementary information (ESI) available. See DOI: https://doi.org/10.1039/d2me00173j

‡ AMPL present address: Technische Universität Berlin, Institut für Biotechnologie, Aufgang 17-1, Level 4, Raum 472, Gustav-Meyer-Allee 25, 13355, Berlin, Germany.

Introduction

Nature showcases a myriad of chemical reactions performed with utmost efficacy and specificity despite the complexity of cells, with the help of macromolecular biological catalysts called enzymes. Their unrivalled efficiency and selectivity have inspired many chemists to explore and push the boundaries of chemical transformations. In this respect, chemical reactions that do not interact nor interfere with native biochemical processes, bio-orthogonal reactions, have attracted a great deal of interest.[1–7] Initially utilised to understand the molecular details of biological processes, bio-orthogonal reactions were diversified to perform *in situ* synthesis in cells.[8] With the advances in bio-orthogonal chemistry, reactions using various transition metal catalysts such as Pd(II)/(0), Ru, Au, or Cu in living cells became promising for biomedical applications.[9–18] Among them, Pd is known for both cross-coupling and bond cleavage reactions in cellular media,[19–21] and has been explored for protein modification or activation,[22,23] cell surface remodeling,[24,25] DNA modification[26] and pro-drug activation.[4,27] Pd(0)/Pd(II) can perform C–O bond cleavage of propargylic or allylic carbamates, ethers, amines, or carbonates in cellular media.[7,11,12,28–33] Hence, it displays therapeutic potential exemplified by its ability to activate pro-drugs or pro-dyes in a controlled manner with minimal toxicity and high specificity. Bradley and co-workers first reported intracellular de-allylation and Suzuki–Miyaura coupling reactions using Pd(0) entrapped polystyrene microspheres of 0.5 μm in diameter.[12] Later, Pd-mediated depropargylation reactions were reported by Chen and coworkers using discrete Pd(II) complexes for protein activation which proved to function better than deallylation reactions.[22] Parallel studies performed by Unciti-Broceta and coworkers with extracellular Pd(0) resins found equivalent results, *i.e.* Pd-mediated depropargylation reactions are faster than deallylations, enabling the activation of the propargyl-protected anticancer drug 5-fluorouracil[34] and propargyloxycarbonyl-protected gemcitabine[38] in cell cultures. They also highlighted the compatibility of these catalysts *in vivo* by locally activating a pro-dye in zebrafish.[34] Weissleder and coworkers reported *in vivo* pro-drug activation of doxorubicin and monomethyl auristatin E by Pd-based nanoparticles thereby inhibiting the growth of solid tumours in mice models opening exciting opportunities to expand *in vivo* palladium chemistry for developing new cancer therapies.[9,32] Further developments from Unciti-Broceta and co-workers on Pd-activatable non-toxic pro-drugs from chemotherapeutics such as doxorubicin, 5-fluorouracil, paclitaxel, *etc.*, widened the scope of new therapies exploiting Pd catalysed pro-drug activation.[11,34–38]

The use of heterogeneous Pd catalysts proved to be advantageous and promising over discrete palladium complexes for *in vivo* pro-drug activation, as it helps overcome the issues of biocompatibility, stability, deactivation, or their sequestration by proteins.[39] However, they are often employed as implants near the tumour tissue which may need to be surgically removed after treatment.[11] To cope with this issue, metal complexes can be loaded into the hydrophobic domain of polymeric scaffolds to form homogeneous systems such as micelles,[40–42] dendrimers,[43] polymerosomes,[44] star polymers,[45] or polymeric nanoparticles.[46–49] They offer the possibility of systemic administration and can be localised to tumour tissues by EPR-mediated passive and RGD or NGR-based active targeting.[50]

Our group has demonstrated that a single amphiphilic polymer with randomly distributed hydrophobic and hydrophilic side-chains folds/collapses in water into a single-chain polymeric nanoparticle (SCPN).[46] These nanoparticles comprise a hydrophobic interior, are in the nanometre-size range, and are completely soluble in water. When ligands capable of binding to transition-metal ions are covalently attached, catalytically-active nanoparticles are obtained, with properties akin to those of metalloenzymes.[46,47,51–53] The hydrophobic interior creates a microenvironment for substrates and catalysts allowing high local concentrations, which results in fast kinetics of the reactions.[53,54] Compared to other polymeric scaffolds, SCPNs have a discrete, small size (5–10 nm), which will benefit tissue permeability and renal clearance.[55–57] SCPNs form a versatile, biocompatible platform that allows easy functionalisation and preparation. Further, they can be readily modified with targeting ligands to improve their localisation in tumour sites for *in vivo* applications.[58] Altogether, SCPNs offer advantages over other reported systems such as heterogeneous Pd(0) resins, offering the possibility of systemic administration, targeted delivery, better penetration into tumour micro-environment and renal clearance. Zimmerman and co-workers reported promising applications of copper and ruthenium-containing SCPNs that perform enzyme-like click reactions or allyl carbamate cleavage in cellular media.[48,49,59] Pd(II)-based SCPNs are a logical extension for *in vivo* prodrug activation owing to their low toxicity but have been less explored in complex media.[51]

We previously evaluated the potential of a first-generation Pd(II)-based SCPN in the depropargylation of a protected rhodamine dye in the cytosol and lysosomal compartments of HeLa cells. Our work revealed that while deprotection was feasible, a boost in the activity and enhancement of the stability of the catalytic system is required to make the system amenable for *in vivo* pro-drug activation.[51] In addition, we found that the polymer's microstructure affected the size and shape of the formed SCPNs and optimised the hydrophobic/hydrophilic balance to attain well-defined, compartmentalised systems with a structured hydrophobic interior.[60] Using the optimised polymer design, we recently observed that the biocompatibility of SCPNs without metals incorporated is excellent and that SCPNs retain their folded, compartmentalised structure in complex media and in the cytoplasm of a variety of cell types.[61] Thus, a profound understanding on how different aspects of the catalytic system affect its efficiency when increasing the complexity of the medium is required to make the step to *in vivo* applications.

We present here our systematic approach to increase the efficiency of Pd(II)-based polymeric nanoparticles for catalysing depropargylation reactions in cellular media by

tuning the different aspects of the catalytic system. We focus on depropargylation reactions as they are reported to be faster than deallylation reactions[34] and various propargyl-protected pro-drugs of clinically used chemotherapeutics are already reported to be non-toxic to cells.[11,34–38] Moreover, depropargylation is cleaner and activates the pro-drug/dye without any toxic side products.[30] Hereto, we use our optimised polymer microstructure and investigate (1) the effect of the metal–ligand combination, (2) the effect of the hydrophobicity of the substrate, (3) the effect of the polymer's microstructure on catalyst's activity and (4) the effect of medium complexity. The best design was then applied in the prodrug activation of the well-established cancer chemotherapeutics paclitaxel (pac), doxorubicin (doc) and 5-fluorouracil (5-FU) in the cell culture medium DMEM. The results indicate that while some prodrugs are activated even in DMEM, a careful balance is required between the substrate and product hydrophobicity. Our bottom-up approach highlights not only the challenges associated with pro-drug activation in complex cellular media but also that a fundamental understanding of all aspects of the applied system is crucial for progress.

Results and discussion

Design and preparation of catalytic polymeric nanoparticles and substrates

The design of the catalytic polymeric nanoparticle system (Fig. 1) is based on our previously studied amphiphilic polymers with a polyacrylamide backbone, grafted Jeffamine

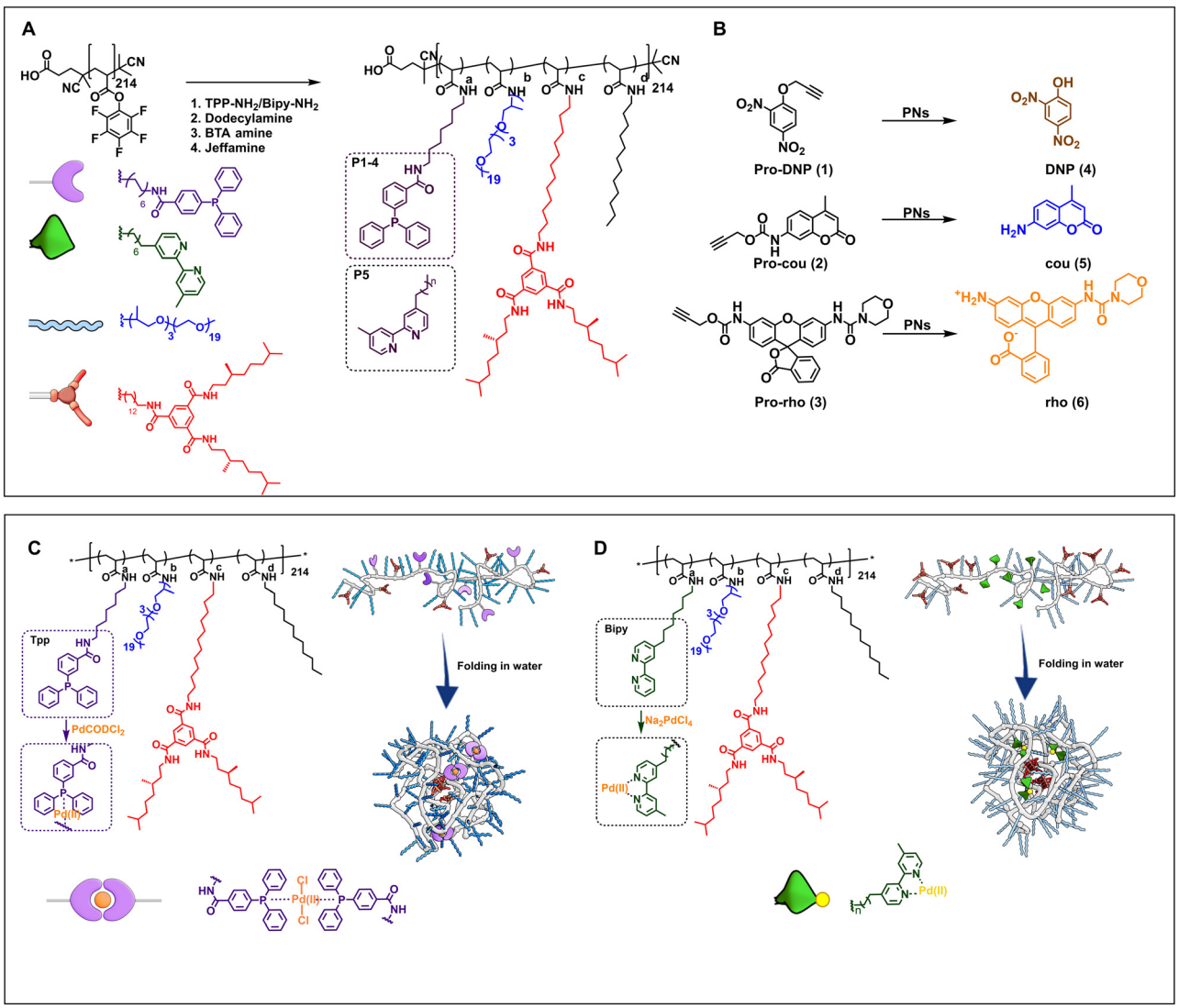

Fig. 1 A) Chemical structures of the amphiphilic polymers **P1**–**P6** functionalized from **pPFPA** in DMF at 50 °C (see ESI† for details). **P1**–**P4** are equipped with triphenylphosphine ligands, **P5** with bipyridine ligands, and **P6** without any ligands. B) Chemical structures of propargyl protected pro-dyes, and representative depropargylation into the corresponding dye, PNs = polymeric nanoparticles in water/PBS/DMEM. Representation of Pd(II) complexation and folding of C) TPP-functionalised polymers, complexation performed in dry and degassed chloroform at R.T. and D) bipy-functionalised polymers, complexation performed in water at R.T. (see ESI† for details).

M-1000 to ensure water solubility, *n*-dodecyl groups to induce a hydrophobic collapse, and benzene-1,3,5-tricarboxamide groups for imparting a secondary structure formation in the nanoparticle's interior *via* hydrogen bonding.[60] In addition, selected ligands are covalently attached to the polymer backbone capable of binding Pd(II). Following the work of Mascareñas, we select triphenylphosphine as this affords active, discrete Pd(II) complexes, also inside HeLa cells.[62] Incorporating phosphine ligands into amphiphilic polymers improves their compatibility with aqueous media, while extending the substrate scope to more hydrophobic molecules. In addition, bipyridine-based ligands were attached to the polymer backbone for reference as we have observed in previous work that these are capable of pro-dye activation in the presence of HeLa cells, albeit with low activity.[51] To obtain an efficient catalytic system, the Pd(II) complex should be well protected inside the hydrophobic pocket and should not leak out into the complex biological environment.

Table 1 summarises the details of the composition of the different polymers **P1–P6**. Amine-functionalised TPP ligand was synthesized starting from 4-(diphenylphosphaneyl)-benzoic acid in two steps (see ESI† for details, Section 3.2–3.3), and amine-functionalised bipyridine ligand was synthesised following a reported procedure (see ESI† for details, Section 3.8–3.10).[63] All polymers were synthesised starting from the same poly(pentafluorophenylacrylate) homopolymer (**pPFPA**, DP = 214, $Đ$ = 1.23, Fig. S21 in the ESI†) by a post-functionalisation approach, using previously developed procedures (Fig. S22–44†).[46] This post-functionalisation approach allows easy functionalisation and ensures a random distribution of the side groups of interest while keeping the same average degree of polymerisation and molar mass dispersity of the polymer backbone.[46,60,64] Polymers **P1–P4** comprised triphenylphosphine (TPP) ligands (~10% in **P1–P3**, ~20% in **P4**), variable amounts of hydrophobic and supramolecular BTA units, and hydrophilic Jeffamine M-1000 (Fig. 1A, Table 1) to vary the microstructure of polymers. **P1** contains 10% BTAs. BTAs attached to a polymer backbone assemble *via* threefold hydrogen-bonding interactions forming *M*-helical stacks.[60] These stacks provide a structured, hydrophobic interior inside the nanoparticles, which is known to enhance the nanoparticle's stability.[61] **P2** contains 5% BTA and 15% dodecyl chains on the backbone, which affords both a structured as well as a compact interior while preventing multichain aggregates due to BTA stacking.[60] **P3** contains 20% dodecyl chains, while **P4** has just the hydrophobicity of the ligand to form a hydrophobic domain inside the particles. The simple chemical structures of **P3** and **P4** highlight the potential of developing easily accessible catalytic polymers for bio-orthogonal catalysis using this approach. **P5** is equipped with 10% bipyridine ligand, 5% BTA, 15% dodecyl, and Jeffamine, similar to the polymer reported previously.[51] A control polymer **P6** without ligands was also prepared to breakdown the complex catalytic system into a simple system which permits physical encapsulation of a Pd(II) complex and study its effect on activity with increasing medium complexity.

Since **P1–P4** are susceptible to oxidation of the TPP ligand, workup and dialysis were performed in degassed solvents. The covalent attachment of the TPP ligands to polymers **P1–P4** was indicated by a resonance peak at −5 ppm in the ^{31}P NMR spectrum (Fig. S36†). Next, TPP functionalised polymers were complexed with Pd(II) using **PdCODCl$_2$** as the palladium source in degassed chloroform under argon atmosphere and highly diluted conditions to minimise intermolecular crosslinking of the particles.[65] We refer to polymer nanoparticles comprising Pd(II) as **P@Pd(II)**. ^{31}P NMR showed that the signal of triphenylphosphine at −5 ppm disappeared, and a new signal downfield between 23–27 ppm formed, confirming the complexation of Pd(II) to TPP (Fig. S45†). We observed minor oxidation of triphenylphosphine in all polymers during complexation as indicated by a small peak at 28 ppm, characteristic of triphenylphosphine oxide.[66] **P1–P4@Pd(II)** were dialysed in chloroform to remove most of the unbound Pd(II) salt. Next, the complexed polymers were formulated into nanoparticles by adding water and sonication for 30 min, followed by equilibration for 1 h. In contrast, bipyridine-based polymer **P5** does not suffer from sensitivity to oxygen and was first formulated to nanoparticles in water by dissolution, followed by complexation of Pd(II) using the water-soluble Pd(II) precursor **Na$_2$PdCl$_4$**. The complexation of **P5** to Pd(II) was followed by UV-vis spectroscopy, where the characteristic absorption of bipyridine was red-shifted after complexation with Pd(II) (Fig. S46†).[51]

Table 1 Overview of the copolymer composition, number-average molecular weight (M_n), and molar mass dispersity ($Đ$) of **pPFP$_{214}$** and **P1–P6**

Polymer	*a*	*b*	*c*	*d*	*n*	$Đ$	$M_{n,SEC}$ (kD)	$M_{n,theoretical}$ (kD)
pPFP$_{214}$						1.23[a]	36.7[a]	51
P1	9	80	11	—	—	1.43[b]	46.8[b]	183
P2	8	68	4	20	—	1.18[b]	42.2[b]	163
P3	9	76	—	15	—	1.28[b]	62.0[b]	158
P4	18	82	—	—	—	1.34[b]	55.4[b]	178
P5	10	66	5	19	6	1.42[b]	46.9[b]	179
P6	—	76	—	24	—	1.41[b]	57.6[b]	164

a–d were determined by ^{19}F NMR. M_n and $Đ$ were measured by SEC. [a] THF, relative to poly(styrene) standards. [b] DMF with 10 mM LiBr, relative to poly(ethylene oxide) standards.

Dynamic light scattering (DLS) studies of **P1–P4@Pd(II)** show hydrodynamic radii (R_H) of 5–6 nm, well in line with previously reported SCPN systems.[51] **P5@Pd(II)**, obtained *via* a slightly different procedure, also showed a R_H of 6 nm (Fig. S47†). The sizes of **P1–P5** based nanoparticles did not change significantly before and after complexation (Fig. S48†). Due to the presence of a small fraction of aggregates after complexation observed in DLS, we adopted the name polymeric nanoparticles instead of SCPNs in this work.

The negative Cotton effect with a minimum at λ = 225 nm in the CD spectra of polymers **P1**, **P2**, and **P5** indicated the presence of *M*-helical BTA aggregates that form threefold hydrogen bonding between the pendant BTA units (Fig. S49†).[67,68] The palladium concentration in all nanoparticles was analysed by MP-AES spectroscopy prior to catalysis studies and the results indicated the presence of ~30–80 Pd(II) ions per particle, meaning that an excess of palladium is trapped in the PNs, which are not able to diffuse out during dialysis (see ESI† for details, Table S1). For all catalytic studies, the total concentration of Pd(II) is kept constant.

The hydrophobicity of the substrates and protecting group plays an essential role during their deprotection by catalytic polymeric nanoparticles, especially in complex media in the presence of competing molecules. The greater the hydrophobicity, the higher is the tendency of substrates to accumulate in hydrophobic reaction space inside the nanoparticles.[53] Therefore, we designed and synthesised a set of propargyl-protected, palladium-activatable pro-dyes based on *o*-dinitrophenol (pro-DNP (**1**)), coumarin (pro-cou (**2**)), and rhodamine (pro-rho, (**3**)) that show different hydrophobicities (for Log*P* values, see Fig. S50†), following reported procedures.[24,30,54] Pro-DNP (**1**) yields DNP (**4**) upon depropargylation. The reaction is monitored using UV-vis spectroscopy at λ = 400 nm.[30] In the case of pro-cou (**2**), the activation to coumarin (**5**) is monitored using fluorescence spectroscopy where the uncaged product has an $\lambda_{ex,max}$ of 370 nm and $\lambda_{em,max}$ of 440 nm when inside the SCPNs.[24] Pro-rho (**3**) yields the fluorescent rhodamine 110 derivative (**6**) upon depropargylation, which has an $\lambda_{ex,max}$ of 495 nm and $\lambda_{em,max}$ of 520 nm.[54]

Activation of pro-dyes in aqueous solution – influence of polymer microstructure and substrate hydrophobicity

We first check the catalytic performance of newly developed Pd(II) loaded TPP-based polymeric nanoparticles in the depropargylation of *O*-propargyl and *N*-propargyloxycarbonyl protected dyes **1–3**. Given these are model reactions toward pro-drug activation in cells, the reaction parameters were chosen to fit with the biological environment. Therefore, reactions were performed in aqueous solutions at physiological temperature (37 °C) and at micromolar concentration of substrates, concentrations used for pro-drug administration *in vivo*.[32] Reactions were monitored using fluorescence/UV-vis spectroscopy in real-time and quantified using HPLC-UV (see ESI† for details). The rate of the reaction was first studied using pro-DNP **1** as substrate in water and PBS. **P1–P4@Pd(II)** nanoparticles were prepared in water or PBS with a concentration of 30 μM Pd(II). To this, a substrate stock solution in DMSO (0.2% in water) was added ([Pro-DNP] = 100 μM). The formation of product DNP was monitored using UV-vis spectroscopy. The kinetic curves in water (Fig. 2B) show saturation after 210 min for **P1@Pd(II)** and around 700 min for **P2–P4@Pd(II)**. For the free catalyst, **$PdCODCl_2$**, no saturation is observed, even after 1200 min. In PBS, **P1–P3@Pd(II)** and **$PdCODCl_2$** show faster formation of DNP, whereas **P4@Pd(II)** showed a similar kinetic profile as in water (Fig. 2C). The results indicate that catalytically active nanoparticles, both in water and PBS, show significantly faster rates compared to free palladium salt **$PdCODCl_2$**. The kinetic data also imply that the exact microstructure of the polymers **P1–P4** has a minor influence on their catalytic activity in water and PBS (Fig. 2B and C).

The free palladium salt **$PdCODCl_2$** shows different behaviour in water and in PBS. In PBS two rate regimes, one fast and one slow, can be observed (Fig. 2C, blue curve). This is similar to what was reported previously for depropargylations by Pd(II) salts in PBS, where it was studied that depropargylation proceeds *via* two phases, one fast and the other slow.[30] The fast phase ends within two turnovers due to product inhibition by the propargylic hydrolytic product, which is followed by a slower reaction phase promoted by Pd(0) nanoparticles formed from Pd(II) in the mixture.[30,69] In contrast, **P1–P4@Pd(II)** nanoparticles catalysed the reaction faster without a slow phase. This could be due to two reasons, a) products formed, which are more hydrophilic than the starting substrate, will have a higher tendency to partition into the aqueous phase, decreasing the chances of product inhibition or b) Pd(0) formed during the cycle is stabilised within the nanoparticles which further allows the continuation of the catalytic cycle.[70] The conversion of pro-DNP after 24 h was between 80–90% in the case of the **P1–P4@Pd(II)**, outperforming the **$PdCODCl_2$** salt where the conversion was only 55%.

The new polymers were further tested on *N*-propargyloxycarbonyl protected dyes pro-cou **2** (hydrophilic) and pro-rho **3** (hydrophobic) to assess the effect of substrate hydrophobicity on the rate of the reaction. The deprotection of pro-cou **2** in water (Fig. 2D) proceeds very slow, reaching only 50% even after 24 h. There is no clear trend between the activity of **P1–P4@Pd(II)** and the free **$PdCODCl_2$** salt (Fig. 2D), albeit that **P1@Pd(II)** seems to be the faster catalyst system. On the other hand, deprotection of pro-rho **3** proceeds very fast, with saturation of the fluorescence increase already after 10 min in the case of **P1@Pd(II)**. The kinetic curves also show that **P4@Pd(II)**, the most hydrophilic nanoparticle with the least hydrophobic content, performed slower compared to others (Fig. 2E), which is also seen for the free **$PdCODCl_2$** salt. Also, it is important to note that **P4@Pd(II)** has ligand incorporation twice compared to **P1–P3@Pd(II)** resulting in higher Pd(II) loading. As a consequence of keeping the Pd(II) concentration

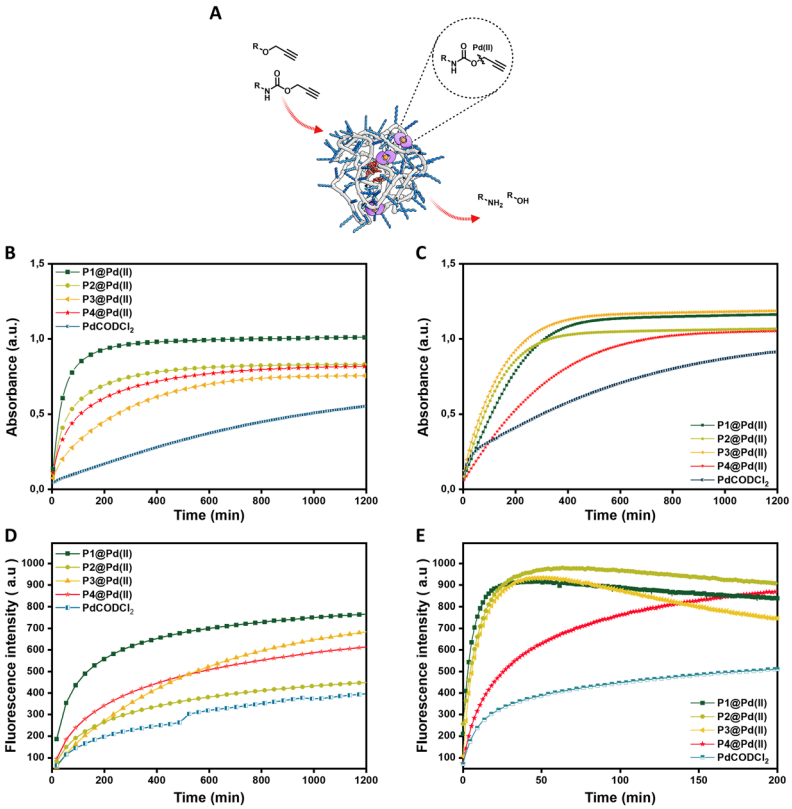

Fig. 2 A) Representation of depropargylation by Pd(II) inside hydrophobic cavity of nanoparticles. Activation of pro-DNP **1** (100 μM) to DNP **4** monitored by UV-vis spectroscopy overtime at λ = 400 nm B) in water C) in PBS D) activation of pro-cou **2** (100 μM) to cou **5** monitored by fluorescence spectroscopy over time λ_{ex} = 370 nm and λ_{em} = 420 nm in water E) activation of pro-rho **3** (100 μM) to rho **6** monitored by fluorescence spectroscopy over time λ_{ex} = 485 nm and λ_{em} = 520 nm in water; all reactions were performed at 37 °C by **P1–P4@Pd(II)** and **$PdCODCl_2$**; in all cases [Pd(II)] = 30 μM.

constant, the concentration of nanoparticles **P4@Pd(II)** in the solution is less, resulting in an overall lesser hydrophobicity to accommodate hydrophobic substrate pro-rho **3**.

Quantification of the conversion with HPLC-UV showed quantitative conversion of pro-rho **3** to rho **6** after 3.3 h using **P1–P3@Pd(II)**. The faster conversion of pro-rho **3** by the more hydrophobic nanoparticles **P1–P3@Pd(II)** suggests that the rate of the deprotection correlates with the hydrophobicity of the substrate, since the rates are significantly slower in the case of pro-DNP **1** and pro-cou **2**. The results also show that **P1@Pd(II)** comprising 10% BTA units outperforms the other nanoparticles in most cases in water. However, the differences between **P1–P3@Pd(II)** are rather small, indicating that as long as the interior of the nanoparticle is sufficiently hydrophobic to accommodate the substrates, the rate of the reaction is similar. We also observed that the product formed tends to aggregate inside the hydrophobic interior, which was inferred from the quenching of the fluorescence over time. Also, **P1@Pd(II)** did not show any deactivation after one cycle, as the addition of more substrate pro-rho **3** resulted in the continuation of reaction to reach full conversion (Fig. S51†). Owing to the fast kinetics of activation of pro-rho substrate **3**, we select this substrate for subsequent experiments in more complex media.

Role of ligand–metal complex in the catalytic activity of nanoparticles

The choice of ligands attached to the polymer backbone to bind Pd(II) plays an important role in the catalytic system design. The ligands should be labile to allow substrate binding but if they are too labile, nucleophiles in the complex media can deactivate the catalyst faster. Therefore, a fine balance on the lability of ligands is necessary to achieve a high turnover in complex media.[69] Here, we compare two ligands, TPP and bipyridine, where TPP is a more labile ligand compared to bipyridine on binding with Pd(II). The labile TPP–Pd(II) complex will allow facile substrate binding and thereby can be more reactive than the stable bipy–Pd(II) complex in water. However, their reactivity in competing environments like in cell culture medium such as DMEM may vary. DMEM medium contains different amino acids such as histidine, cysteine, methionine *etc.* that are known to complex with Pd(II), with a higher affinity to sulphur-containing amino acids.[73] Therefore, these amino acids can interact with Pd(II) displacing the ligands, hence deactivating the catalyst. Here, we studied the effect of TPP and bipyridine on the catalytic activity of polymer nanoparticles in the depropargylation of pro-rho **3** (Fig. 3) in both water and

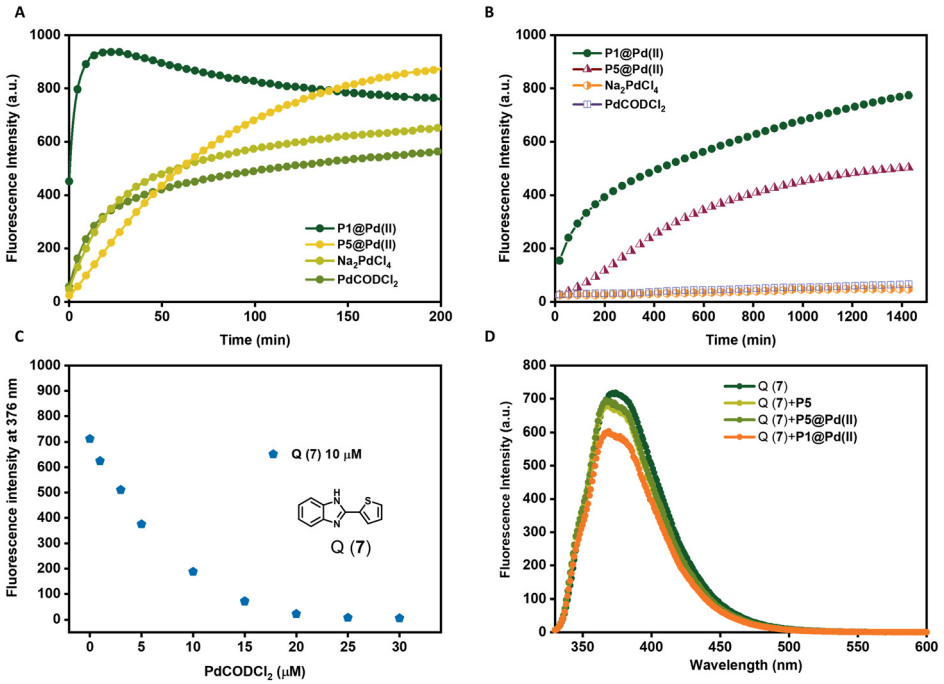

Fig. 3 Activation of pro-rho **3** (100 μM) monitored by fluorescence spectroscopy over time λ_{ex} = 485 nm and λ_{em} = 520 nm A) in water, B) in DMEM all reactions were performed at 37 °C by **P1@Pd(II)**, **P5@Pd(II)**, **Na_2PdCl_4** and **$PdCODCl_2$**, [Pd(II)] = 30 μM in water and [Pd(II)] = 100 μM in DMEM. C) Fluorescent quenching of *Q*(**7**) (10 μM) with increasing **$PdCODCl_2$** concentration (1–30 μM). D) Pd(II) leaching test, emission of *Q*(**7**) at λ_{ex} = 320 nm in the presence of **P1&P5@Pd(II)** filtrate solutions [*Q*(**7**)] = 10 μM, [*P*] = 0.25 mg mL^{-1}, [Pd(II)] = 30 μM (before filtration), *T* = 20 °C, in H_2O.

DMEM. **P1@Pd(II)** and **P5@Pd(II)** were compared, as well as their Pd(II) precursors **$PdCODCl_2$** and **Na_2PdCl_4**.

In water, TPP-based **P1@Pd(II)** performed the depropargylation faster, reaching full conversion in 3.3 h, compared to bipy-based **P5@Pd(II)** which was slower and did not reach full conversion even after 16 h (Fig. 3A, Table 2). This suggests that the TPP–Pd(II) complex accelerates the depropargylation more efficiently than the bipy–Pd(II) complex. Also in DMEM, TPP-based **P1@Pd(II)** performed slightly better than bipy-based **P5@Pd(II)** (Fig. 3B, Table 2). Interestingly the free Pd salts **$PdCODCl_2$** and **Na_2PdCl_4** showed a decent activity in water (Fig. 3A) but were fully deactivated in the presence of DMEM (Fig. 3B). This result suggests that TPP and bipy ligands when bound to Pd(II) prevent fast deactivation, and the presence of ligands is essential to retain the catalytic activity of Pd(II) catalysts. However, there is a significant rate decrease when the reactions are conducted in DMEM compared to water.

Table 2 Conversion of pro-rho **3** (100 μM) to rho **6** monitored by HPLC-UV

Catalyst	Medium*	Pd(II)* mol%	Conversion	
P1@Pd(II)	Water	30	100%[a]	
	DMEM	100	29[b]	78%[c]
P5@Pd(II)	Water	30	56%[a]	86%[b]
	DMEM	100	28%[c]	56%[d]
$PdCODCl_2$	Water	30	49%[a]	66%[b]
	DMEM	100	n.d.[c]	n.d.[d]
Na_2PdCl_4	Water	30	56%[a]	70%[b]
	DMEM	100	n.d.[c]	n.d.[d]

[a] 3.3 h. [b] 16 h. [c] 24h. [d] 48 h. n.d. = not determined as no conversion was observed in DMEM during fluorescence kinetic experiments. Reactions performed at *T* = 37 °C. *Concentration of Pd(II) and medium of reaction as specified.

To get more insight into this, we designed an experiment to test the leaching of Pd(II) catalysts from the nanoparticles. **P1@Pd(II)** and **P5@Pd(II)** in water ([Pd(II)] = 30 μM, [**P1**/**P2**] = 0.25 mg mL^{-1}) were centrifuged with centrifugal filters with a molecular weight cutoff of 50 kD, to separate the polymers from the solution. The solution was then tested for the presence of leached-out Pd(II) using an imidazole derivative-based dye *Q*(**7**), which exhibits fluorescence quenching in the presence of Pd(II) (Fig. 3C).[71]

The concentration of *Q*(**7**) was fixed at 10 μM while mixing with the filtrate solution (final [Pd(II)] = 25 μM, if there is complete leaching of Pd(II)). Total quenching of *Q*(**7**) fluorescence will be observed if 100% Pd(II) is leached out. In the case of **P5@Pd(II)**, there was no significant reduction in the emission of **7** and the result was similar to the control polymer **P5** without Pd(II) (Fig. 3D). This indicates that there is no significant leaching of Pd(II) and that the ligand–Pd(II) complex is very stable in **P5@Pd(II)**. However, for **P1@Pd(II)** there was a slight reduction in fluorescence intensity, which corresponded to ~4–8% of Pd(II) leaching out. Still, the overall loss of Pd(II) is rather low. We conclude from the leaching experiment that our design of ligand-based

nanoparticles ensures good catalyst encapsulation, while limiting its deactivation compared to free Pd(II) catalysts. Also, the activity of **P1@Pd(II)** in complex media is improved compared to our Pd(II)-SCPNs reported earlier, even at lower catalyst loading (Fig. 3B).[51] Likely, the reduction in activity when going from water to DMEM is related to sequestration of Pd(II) by constituents of the DMEM medium.

Complexity of the system *vs.* catalytic activity in different media

Polymeric nanoparticles perform functions utilising the hydrophobic compartment where both hydrophobic substrates and catalysts can accumulate, accelerating reactions in the aqueous medium. If the catalysts are sufficiently hydrophobic, the catalytic system can be simplified by encapsulation of the catalyst in a simple and easily accessible amphiphilic polymer, which can perform the same function. If such a system remains active in a complex medium, many synthesis steps can potentially be avoided, making the applicability of such nanoparticles more versatile. In order to test this, we designed, evaluated, and compared four systems: a) a simple Pd(II) salt encapsulated in amphiphilic polymers (**P6@PdCODCl$_2$**); b) phosphine–Pd(II) complex encapsulated in amphiphilic polymers (**P6@TPPPd$_2$Cl$_2$**); c) phosphine–Pd(II) complex covalently attached to polymer (**P1@Pd(II)**); and d) the free **PdCODCl$_2$** as a reference.

The four catalytic systems were compared for their efficiency to catalyze the depropargylation reaction of pro-rho **3** in water and DMEM medium (Fig. 4). In water (Fig. 4A), a steep increase in the fluorescence intensity is observed for all systems except for free **PdCODCl$_2$**. Although **P1@Pd(II)** is by far the fastest catalyst, covalent attachment of the catalyst to the polymer backbone is not necessary to achieve conversion in a reasonable time scale. This indicates that the free catalysts either accumulate in the hydrophobic pocket or get trapped inside the polymer microstructure, which then aids in the solubilisation of substrates converting them to products. Remarkably, in DMEM (Fig. 4B), the covalent attachment of the Pd(II) ligand to the polymer backbone as in **P1@Pd(II)** is crucial to retain catalytic activity. In all other catalysts systems, activity is strongly decreased as in **P6@TPPPd$_2$Cl$_2$** or almost completely lost (free **PdCODCl$_2$** and **P6@PdCODCl$_2$**). Thus, encapsulation of the Pd(II) salt does not provide sufficient protection to the catalysts as it is likely not hydrophobic enough to remain inside the hydrophobic reaction pocket (Fig. 4B). The TPP–Pd(II) complex is more hydrophobic, due to which the encapsulated complex performs slightly better than Pd(II) salts in DMEM (Fig. 4B). All in all, our results show that an increase in the complexity of the system, aids the catalyst activity when the reaction is performed in competitive media such as DMEM (Fig. 4C).

Activation of anti-cancer pro-drugs

TPP-based **P1@Pd(II)** shows promising activity in complex media such as DMEM. Therefore, we selected **P1@Pd(II)** for evaluating the ability to activate anticancer pro-drugs. Pro-drugs based on 5-fluorouracil, paclitaxel, and doxorubicin (Scheme 1) with different hydrophobicities (for Log*P* values,

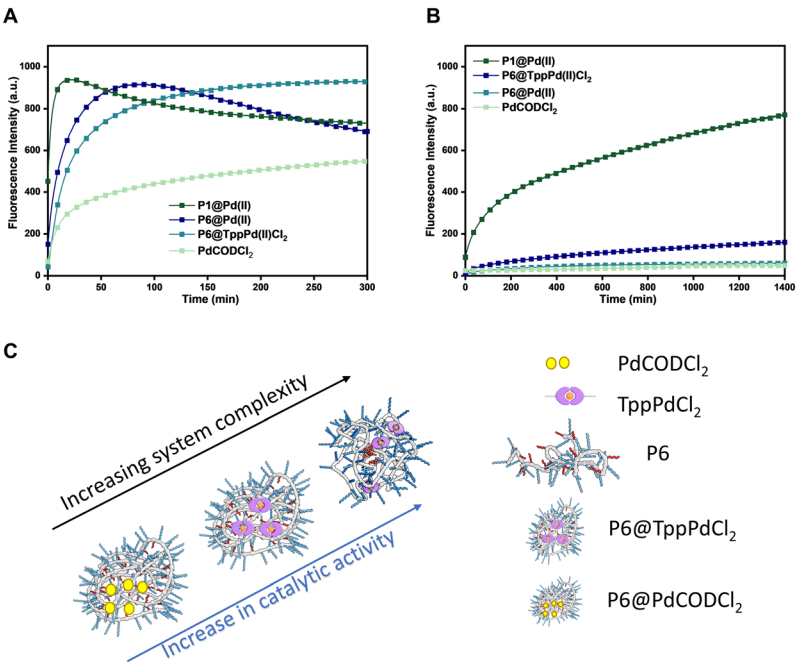

Fig. 4 Activation of pro-rho **3** (100 μM) by **P1@Pd(II)**, **P6@PdCODCl$_2$**, **P6@TppPd(II)Cl$_2$** and **PdCODCl$_2$** in A) water B) DMEM monitored by fluorescence spectroscopy over time λ_{ex} = 485 nm and λ_{em} = 520 nm; all reactions were performed at 37 °C, [Pd(II)] = 30 μM in water and [Pd(II)] = 100 μM in DMEM. C) Representation of the four catalytic systems with increasing system complexity and their catalytic activity with increasing medium complexity.

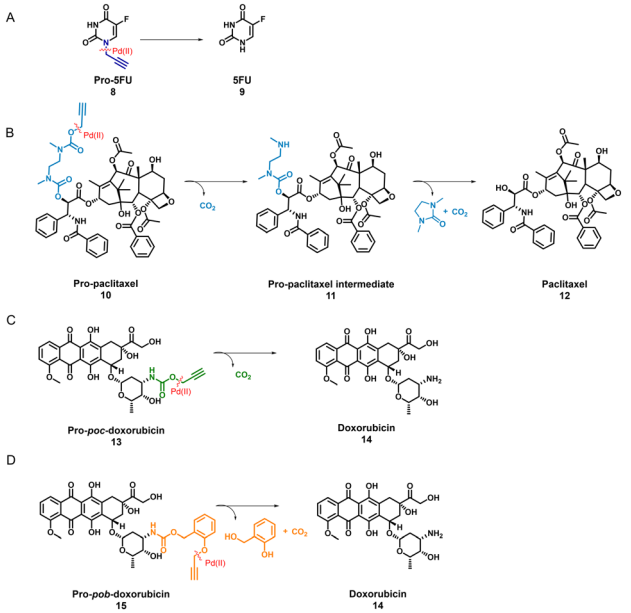

Scheme 1 Scheme for pro-drug activation catalysed by Pd(II) catalyst on 4 different anti-cancer pro-drugs (A) pro-5FU to 5-FU (B) pro-paclitaxel to paclitaxel (C) pro-*poc*-doxorubicin to doxorubicin and (D) pro-*pob*-doxorubicin to doxorubicin.

see Fig. S50†), and protecting groups were chosen as substrates for the activation to find the best substrate suitable for the nanoparticle-based catalytic system. Masking of these drugs with Pd labile protecting groups reduces their cytotoxicity but on activation converts to corresponding drugs that induce cell death. The activation pathway of all four pro-drugs (Scheme 1) starts with depropargylation mediated by Pd(II). Catalytic reactions were performed with **P1@Pd(II)** and the results were compared to those obtained by free $\mathbf{PdCODCl_2}$ salt. The qualitative conversion was monitored using HPLC-UV/MS.

Pro-5FU **8** is a very hydrophilic pro-drug of the widely used therapeutic drug 5-FU **9** and is of interest to test if it is compatible with the nanoparticle-based catalytic system. Pro-5FU activation was tested in water, PBS, and DMEM. In water, **P1@Pd(II)** activates pro-5FU in 16 h when equimolar concentrations of Pd(II) were used. This is significantly faster than when free $\mathbf{PdCODCl_2}$ is applied, where no full conversion is observed after 16 h. The same trend was observed when using PBS (Fig. 5A). When the amount of Pd(II) was reduced to 30 mol% in PBS, the reaction progressed slower, and no significant difference between free $\mathbf{PdCODCl_2}$ and **P1@Pd(II)** was observed (Fig. 5B). In DMEM, the trend was difficult to observe by UV/MS detection due to the presence of its components that influence detection. However, pro-5FU activation proceeded at a slow rate, and full conversion was not achieved, not even at an equimolar concentration of Pd(II) (Fig. S55A†). These findings suggest that hydrophilic pro-drugs are indeed suitable for nanoparticle-based catalytic systems where the reaction proceeds, even if slowly, at catalytic amounts of Pd(II), which is promising for future development of targeted cancer therapy where these polymeric nanoparticles can be decorated with tumour-targeting ligands.

In contrast to pro-5FU, pro-paclitaxel is a very large and hydrophobic drug and therefore an interesting substrate to be tested. Due to its high hydrophobicity, the parent drug paclitaxel is usually delivered using nanoplatforms such as micelles, or liposomes for clinical therapy.[72] During activation, depropargylation of the terminal propargyl group of pro-paclitaxel can be followed by the disappearance of pro-paclitaxel **10**, resulting in an intermediate **11** which should undergo intramolecular cyclisation to form paclitaxel **12**. In PBS, complete disappearance of **10** was observed within 9 h in case of reaction catalysed by **P1@Pd(II)** (30 mol% Pd(II) with respect to substrate) while this was not the case for the $\mathbf{PdCODCl_2}$ salt (Fig. 6A and B). This shows that substrate and catalyst accumulation indeed result in good kinetics in the case of **P1@Pd(II)**. However, in both cases, the formed intermediate **11** was stable, eluted earlier, and did not further convert to paclitaxel **12**, not even after 48 h (Fig. 6A and B). In DMEM, the $\mathbf{PdCODCl_2}$ salt did not activate pro-paclitaxel both at 30 mol% and 100 mol% catalyst concentrations (Fig. 6A and D). In the case of the **P1@Pd(II)**, **11** and **12** were formed in trace amounts within 50 min although full conversion was not achieved even after 48 h (Fig. 6C). The HPLC trace indicates two peaks corresponding to paclitaxel

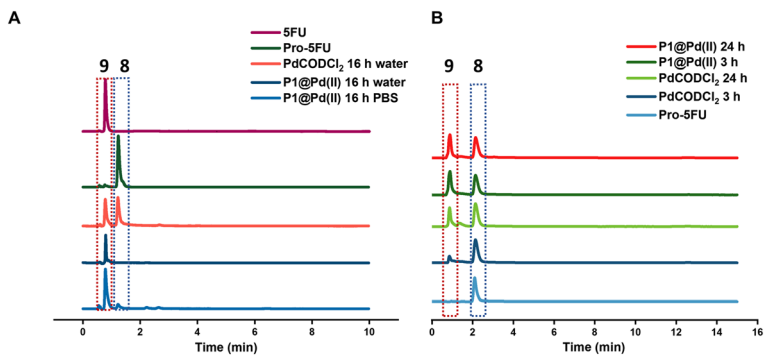

Fig. 5 Pro-5FU activation A) in water and PBS [Pd(II)] = 100 μM, [pro-5FU] = 100 μM (HPLC-UV detection 265 nm) B) in PBS(HPLC-MS). [Pd(II)] = 30 μM, [pro-5FU] = 100 μM, all reactions were performed at 37 °C.

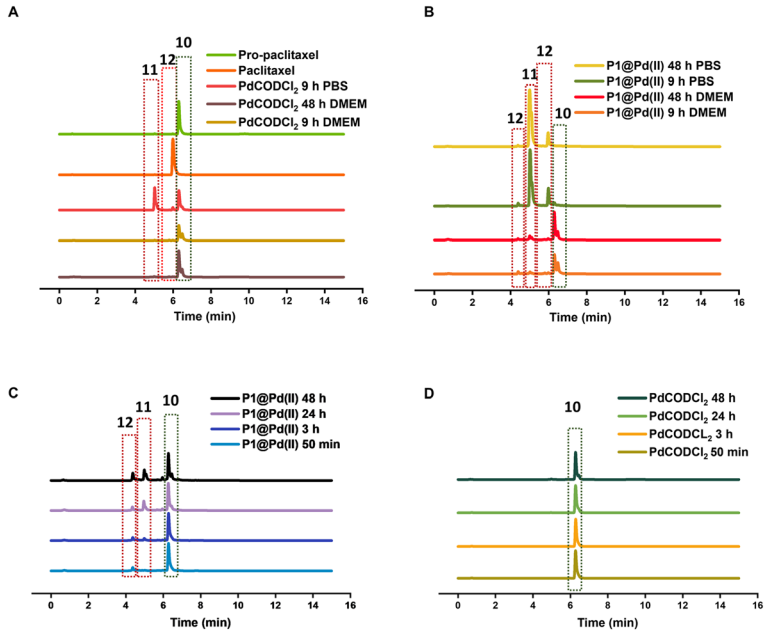

Fig. 6 HPLC-MS chromatogram of paclitaxel activation by A) **PdCODCl$_2$** in PBS and DMEM B) **P1@Pd(II)** in PBS and DMEM. [Pd(II)] = 30 μM, [pro-paclitaxel] = 100 μM C) by **P1@Pd(II)** in DMEM D) by **PdCODCl$_2$** in DMEM, [Pd(II)] = 100 μM, [pro-paclitaxel] = 100 μM monitored by HPLC-MS overtime, all reactions were performed at 37 °C.

(confirmed by MS) in the presence of polymers which is more obvious in DMEM medium. We hypothesise that the paclitaxel present in the hydrophobic cavity of the nanoparticles and paclitaxel in solution elute at different time points. These results indicate that pro-drugs/activated drugs with high hydrophobicity are stabilised in the hydrophobic pocket and are likely less suitable for designing nanoparticle-based pro-drug activation in cells.

We also tested pro-*poc*-doxorubicin **13** and pro-*pob*-doxorubicin **15** in water. The **PdCODCl$_2$** salt activated **13** faster than **P1@Pd(II)** because complete disappearance of **13** and **15** was observed after 16 h with **PdCODCl$_2$** salt while in the case of **P1@Pd(II)** the pro-drug still remained in the reaction mixture (Fig. S55B and C†). Even though the peaks are not clearly resolved in HPLC chromatogram for the reaction catalysed by **P1@Pd(II)**, substrates **13** and **15** can be detected together with product **14**. Easily cleavable propargyl carbamate protecting group and hydrophilicity together makes these prodrugs more prone to activation without the presence of nanoparticles. This shows that our nanoparticle-based catalytic system does not improve the activation of dox-based pro-drugs dramatically. Therefore, careful selection of new pro-drugs with optimum hydrophobicity and stable protecting groups is necessary to further develop a polymeric nanoparticle-based pro-drug activation strategy. A good balance of pro-drug and drug hydrophobicity is required for this system for efficient efflux of drugs to induce cell death.

Conclusions

In conclusion, we have evaluated different aspects of the SCPN-based catalytic system to improve its performance in complex cellular media. Our findings confirmed that the polymer microstructure has only a minor influence on the catalytic activity of nanoparticles when there is enough hydrophobicity in the pocket to accommodate substrates. The most crucial aspect of the design is the selection of the ligand–metal complex, where an optimal balance of stability and activity is required. TPP-based **P1@Pd(II)** nanoparticles were the most efficient and activated pro-rho to reach full conversion in 3.3 h at 30 mol% catalyst loading in water. Notably, unlike free Pd(II) catalysts, both bipy-based and TPP-based catalytic systems retained their activity in the cell culture medium DMEM, and **P1@Pd(II)** activated pro-rho reaching 78% conversion in 48 h at 100 mol% catalyst loading. The catalyst loadings used in this work are lower compared to other reports in the field, highlighting the efficiency of our system to perform at low Pd(II) concentrations in complex media. In addition, Pd(II) leaching studies revealed that 4–8% of Pd(II) is lost from the hydrophobic interior in the case of TPP-based system **P1@Pd(II)**, while no leaching was observed in the case of bipy-based **P5@Pd(II)**. This confirmed that our designed nanoparticles are efficient in preventing the leaching of Pd(II), which is critical for *in vivo* applications as free Pd(II) ions can cause off-target toxicity and decrease the efficiency of catalysts. Careful deconstruction of the catalytic system revealed that the design can be modified to be more synthetically accessible depending on the medium complexity. Physical encapsulation of catalysts in an amphiphilic polymer proved to be sufficient for activity in less complex media such as water and PBS.

TPP-based nanoparticles proved to be the best in terms of activity, which was further evaluated for pro-drug activation of pro-5FU, pro-paclitaxel, and pro-doxorubicin in relevant media. The rate of pro-drug activation in water is accelerated

efficiently by nanoparticles, conversion in complex media was more sensitive to the protection group and the substrate polarity. The activation of pro-5FU and pro-paclitaxel in PBS by our designed system is as efficient as Pd(0) resins and Pd-nanosheets, respectively, that are already reported to work efficiently near tumour tissue, which highlights the possibility of translating our system for *in vivo* applications.[36,38] The catalytic efficiency of TPP-based nanoparticles in complex media could not be directly compared to other studies, as often these are performed in cells instead of cell culture media. However, hydrophobic drugs such as paclitaxel tend to accumulate in the hydrophobic pocket of nanoparticles, which can affect catalyst performance by product inhibition while also limiting its bioactivity. Overall, our results indicated that hydrophobic substrates in combination with nanoparticles accelerated reaction rates, but a good balance of substrate and product hydrophobicity is required for further improvements and new designs. The ligand-based approach is essential to retain the catalytic activity in a complex medium while screening of new ligand–metal complexes that can withstand nucleophiles in complex media is necessary to further improve the efficiency of nanoparticles. We believe that careful evaluation of the cause of poor catalyst performance is more meaningful than increasing catalyst loading for cellular studies. In short, our findings can aid in the development of more efficient synthetically accessible, stable, and active catalytic nanoparticles, which, when combined with improved substrate design, can greatly increase the potential for *in vivo* pro-drug activation.

Author contributions

The manuscript was written through contributions of all authors. All authors have given approval to the final version of the manuscript.

Conflicts of interest

There are no conflicts to declare.

Acknowledgements

This work is financed by the European Union's Horizon 2020 research and innovation program under the Marie Sklodowska-Curie Grant Agreement no. 765497 (THERACAT). AMPL and AUB thank EPSRC (EP/N021134/1) for funding. We would like to acknowledge Vishnu Sureshkumar and Alperen Uslu for help with MP-AES measurements, Dr. Gijs ter Huurne for BTA–NH_2, and ICMS animation studio for artwork. Xianwen Lou is acknowledged for help with LC–MS.

Notes and references

1 E. M. Sletten and C. R. Bertozzi, *Acc. Chem. Res.*, 2011, **44**, 666–676.
2 J. A. Prescher and C. R. Bertozzi, *Nat. Chem. Biol.*, 2005, **1**, 13–21.
3 T. Liang, Z. Chen, H. Li and Z. Gu, *Trends Chem.*, 2022, **4**, 157–168.
4 W. Wang, X. Zhang, R. Huang, C.-M. Hirschbiegel, H. Wang, Y. Ding and V. M. Rotello, *Adv. Drug Delivery Rev.*, 2021, **176**, 113893.
5 M. O. N. van de L'Isle, M. C. Ortega-Liebana and A. Unciti-Broceta, *Curr. Opin. Chem. Biol.*, 2021, **61**, 32–42.
6 B. Lozhkin and T. R. Ward, *Bioorg. Med. Chem.*, 2021, **45**, 116310.
7 Y. Bai, J. Chen and S. C. Zimmerman, *Chem. Soc. Rev.*, 2018, **47**, 1811–1821.
8 C. R. Bertozzi, *Acc. Chem. Res.*, 2011, **44**(9), 651–653.
9 M. A. Miller, H. Mikula, G. Luthria, R. Li, S. Kronister, M. Prytyskach, R. H. Kohler, T. Mitchison and R. Weissleder, *Nano Lett.*, 2018, **12**, 12814–12826.
10 A. M. Pérez-López, B. Rubio-Ruiz, V. Sebastián, L. Hamilton, C. Adam, T. L. Bray, S. Irusta, P. M. Brennan, G. C. Lloyd-Jones, D. Sieger, J. Santamaría and A. Unciti-Broceta, *Angew. Chem.*, 2017, **129**, 12722–12726.
11 T. L. Bray, M. Salji, A. Brombin, A. M. Pérez-López, B. Rubio-Ruiz, L. C. A. Galbraith, E. E. Patton, H. Y. Leung and A. Unciti-Broceta, *Chem. Sci.*, 2018, **9**, 7354–7361.
12 R. M. Yusop, A. Unciti-Broceta, E. M. V. Johansson, R. M. Sánchez-Martín and M. Bradley, *Nat. Chem.*, 2011, **3**, 239–243.
13 C. Vidal, M. Tomás-Gamasa, P. Destito, F. López and J. L. Mascareñas, *Nat. Commun.*, 2018, **9**, 1–9.
14 T. Völker, F. Dempwolff, P. L. Graumann and E. Meggers, *Angew. Chem., Int. Ed.*, 2014, **53**, 10536–10540.
15 C. Vidal, M. Tomás-Gamasa, A. Gutiérrez-González and J. L. Mascarenas, *J. Am. Chem. Soc.*, 2019, **141**, 5125–5129.
16 T. Völker and E. Meggers, *Curr. Opin. Chem. Biol.*, 2015, **25**, 48–54.
17 M. Martínez-Calvo and J. L. Mascareñas, *Coord. Chem. Rev.*, 2018, **359**, 57–79.
18 M. Tomás-Gamasa, M. Martínez-Calvo, J. R. Couceiro and J. L. Mascarenãs, *Nat. Commun.*, 2016, **7**, 1–10.
19 J. Li and P. R. Chen, *ChemBioChem*, 2012, **13**, 1728–1731.
20 C. P. Ramil and Q. Lin, *Chem. Commun.*, 2013, **49**, 11007–11022.
21 P. K. Sasmal, C. N. Streu and E. Meggers, *Chem. Commun.*, 2013, **49**, 1581–1587.
22 J. Li, J. Yu, J. Zhao, J. Wang, S. Zheng, S. Lin, L. Chen, M. Yang, S. Jia, X. Zhang and P. R. Chen, *Nat. Chem.*, 2014, **6**, 352–361.
23 J. M. Chalker, G. J. L. Bernardes and B. G. Davis, *Acc. Chem. Res.*, 2011, **44**, 730–741.
24 J. Wang, B. Cheng, J. Li, Z. Zhang, W. Hong, X. Chen and P. R. Chen, *Angew. Chem., Int. Ed.*, 2015, **54**, 5364–5368.
25 C. D. Spicer, T. Triemer and B. G. Davis, *J. Am. Chem. Soc.*, 2012, **134**, 800–803.
26 L. Lercher, J. F. McGouran, B. M. Kessler, C. J. Schofield and B. G. Davis, *Angew. Chem., Int. Ed.*, 2013, **52**, 10553–10558.
27 J. Li and P. R. Chen, *Nat. Chem. Biol.*, 2016, **12**, 129–137.

28 Z. Chen, H. Li, Y. Bian, Z. Wang, G. Chen, X. Zhang, Y. Miao, D. Wen, J. Wang, G. Wan, Y. Zeng, P. Abdou, J. Fang, S. Li, C. J. Sun and Z. Gu, *Nat. Nanotechnol.*, 2021, **16**, 933–941.
29 S. V. Chankeshwara, E. Indrigo and M. Bradley, *Curr. Opin. Chem. Biol.*, 2014, **21**, 128–135.
30 S. E. Coelho, F. S. S. Schneider, D. C. de Oliveira, G. L. Tripodi, M. N. Eberlin, G. F. Caramori, B. de Souza and J. B. Domingos, *ACS Catal.*, 2019, **9**, 3792–3799.
31 J. Konč, V. Sabatino, E. Jiménez-Moreno, E. Latocheski, L. R. Pérez, J. Day, J. B. Domingos and G. J. L. Bernardes, *Angew. Chem.*, 2022, **61**, e2021135.
32 M. A. Miller, B. Askevold, H. Mikula, R. H. Kohler, D. Pirovich and R. Weissleder, *Nat. Commun.*, 2017, **8**, 1–13.
33 R. C. Brewster, E. Klemencic and A. G. Jarvis, *J. Inorg. Biochem.*, 2021, **215**, 111317.
34 J. T. Weiss, J. C. Dawson, K. G. Macleod, W. Rybski, C. Fraser, C. Torres-Sánchez, E. E. Patton, M. Bradley, N. O. Carragher and A. Unciti-Broceta, *Nat. Commun.*, 2014, **5**, 1–9.
35 A. M. Pérez-López, B. Rubio-Ruiz, T. Valero, R. Contreras-Montoya, L. Á. De Cienfuegos, V. Sebastián, J. Santamaría and A. Unciti-Broceta, *J. Med. Chem.*, 2020, **63**, 9650–9659.
36 C. Adam, A. M. Pérez-López, L. Hamilton, B. Rubio-Ruiz, T. L. Bray, D. Sieger, P. M. Brennan and A. Unciti-Broceta, *Chem. – Eur. J.*, 2018, **24**, 16783–16790.
37 J. T. Weiss, N. O. Carragher and A. Unciti-Broceta, *Sci. Rep.*, 2015, **5**, 1–7.
38 J. T. Weiss, J. C. Dawson, C. Fraser, W. Rybski, C. Torres-Sánchez, M. Bradley, E. E. Patton, N. O. Carragher and A. Unciti-Broceta, *J. Med. Chem.*, 2014, **57**, 5395–5404.
39 G. Y. Tonga, Y. Jeong, B. Duncan, T. Mizuhara, R. Mout, R. Das, S. T. Kim, Y.-C. C. Yeh, B. Yan, S. Hou and V. M. Rotello, *Nat. Chem.*, 2015, **7**, 597–603.
40 S. Tevet, S. S. Wagle, G. Slor and R. J. Amir, *Macromolecules*, 2021, **54**, 11419–11426.
41 M. Cortes-Clerget, N. Akporji, J. Zhou, F. Gao, P. Guo, M. Parmentier, F. Gallou, J. Y. Berthon and B. H. Lipshutz, *Nat. Commun.*, 2019, **10**, 1–10.
42 S. Wallace, E. P. Balskus, M. Cortes-Clerget, N. Akporji, J. Zhou, F. Gao, P. Guo, M. Parmentier, F. Gallou, J. Y. Berthon and B. H. Lipshutz, *Angew. Chem., Int. Ed.*, 2016, **55**, 6023–6027.
43 C. Deraedt, N. Pinaud and D. Astruc, *J. Am. Chem. Soc.*, 2014, **136**, 12092–12098.
44 K. T. Kim, J. J. L. M. Cornelissen, R. J. M. Nolte and J. C. M. van Hest, *Adv. Mater.*, 2009, **21**, 2787–2791.
45 Q. Lu, S. Bai, Z. Chen, N. Zheng, X. Feng and Y. Bai, *ACS Mater. Lett.*, 2020, **2**, 89–94.
46 Y. Liu, T. Pauloehrl, S. I. Presolski, L. Albertazzi, A. R. A. Palmans and E. W. Meijer, *J. Am. Chem. Soc.*, 2015, **137**, 13096–13106.
47 M. Artar, T. Terashima, M. Sawamoto, E. W. Meijer and A. R. A. Palmans, *J. Polym. Sci., Part A: Polym. Chem.*, 2014, **52**, 12–20.
48 J. Chen, J. Wang, Y. Bai, K. Li, E. S. Garcia, A. L. Ferguson and S. C. Zimmerman, *J. Am. Chem. Soc.*, 2018, **140**, 13695–13702.
49 J. Chen, J. Wang, K. Li, Y. Wang, M. Gruebele, A. L. Ferguson and S. C. Zimmerman, *J. Am. Chem. Soc.*, 2019, **141**, 9693–9700.
50 S. Kunjachan, R. Pola, F. Gremse, B. Theek, J. Ehling, D. Moeckel, B. Hermanns-Sachweh, M. Pechar, K. Ulbrich, W. E. Hennink, G. Storm, W. Lederle, F. Kiessling and T. Lammers, *Nano Lett.*, 2014, **14**, 972–981.
51 Y. Liu, S. Pujals, P. J. M. Stals, T. Paulöhrl, S. I. Presolski, E. W. Meijer, L. Albertazzi and A. R. A. Palmans, *J. Am. Chem. Soc.*, 2018, **140**, 3423–3433.
52 T. Terashima, T. Mes, T. F. A. A. de Greef, M. A. J. J. Gillissen, P. Besenius, A. R. A. Palmans and E. W. Meijer, *J. Am. Chem. Soc.*, 2011, **133**, 4742–4745.
53 M. Artar, E. R. J. Souren, T. Terashima, E. W. Meijer and A. R. A. Palmans, *ACS Macro Lett.*, 2015, **4**, 1099–1103.
54 Y. Liu, P. Turunen, B. F. M. de Waal, K. G. Blank, A. E. Rowan, A. R. A. Palmans and E. W. Meijer, *Mol. Syst. Des. Eng.*, 2018, **3**, 609–618.
55 Z. Li, C. Xiao, T. Yong, Z. Li, L. Gan and X. Yang, *Chem. Soc. Rev.*, 2020, **49**, 2273–2290.
56 J. Liu, M. Guo and C. Chen, *Adv. Drug Delivery Rev.*, 2022, **186**, 114318.
57 R. van der Meel, E. Sulheim, Y. Shi, F. Kiessling, W. J. M. Mulder and T. Lammers, *Nat. Nanotechnol.*, 2019, **14**, 1007–1017.
58 X. Zhang, R. Huang, S. Gopalakrishnan, R. Cao-Milán and V. M. Rotello, *Trends Chem.*, 2019, **1**, 90–98.
59 E. S. Garcia, T. M. Xiong, A. Lifschitz and S. C. Zimmerman, *Polym. Chem.*, 2021, **12**, 6755–6760.
60 G. M. ter Huurne, L. N. J. de Windt, Y. Liu, E. W. Meijer, I. K. Voets and A. R. A. Palmans, *Macromolecules*, 2017, **50**(21), 8562–8569.
61 L. Deng, L. Albertazzi and A. R. A. Palmans, *Biomacromolecules*, 2022, **23**, 326–338.
62 M. Martínez-Calvo, J. R. Couceiro, P. Destito, J. Rodríguez, J. Mosquera and J. L. Mascareñas, *ACS Catal.*, 2018, **8**, 6055–6061.
63 U. Schatzschneider and J. K. Barton, *J. Am. Chem. Soc.*, 2004, **126**, 8630–8631.
64 M. Eberhardt, R. Mruk, R. Zentel and P. Théato, *Eur. Polym. J.*, 2005, **41**(7), 1569–1575.
65 J. Willenbacher, O. Altintas, V. Trouillet, N. Knöfel, M. J. Monteiro, P. W. Roesky and C. Barner-Kowollik, *Polym. Chem.*, 2015, **6**, 4358–4365.
66 D. F. Shriver and P. W. Atkins, *Inorganic chemistry*, Oxford University Press, Oxford, 3rd edn, 1999.
67 M. A. J. Gillissen, T. Terashima, E. W. Meijer, A. R. A. Palmans and I. K. Voets, *Macromolecules*, 2013, **46**, 4120–4125.
68 E. Huerta, P. J. M. Stals, E. W. Meijer and A. R. A. Palmans, *Angew. Chem.*, 2013, **125**, 2978–2982.
69 E. Latocheski, G. M. Dal Forno, T. M. Ferreira, B. L. Oliveira, G. J. L. Bernardes and J. B. Domingos, *Chem. Soc. Rev.*, 2020, **49**, 7710–7729.
70 S. U. Son, Y. Jang, K. Y. Yoon, E. Kang and T. Hyeon, *Nano Lett.*, 2004, **4**(6), 1147–1151.

71 S. Suresh, N. Bhuvanesh, A. Raman, P. Sugumar, D. Padmanabhan, S. Easwaramoorthi, M. N. Ponnuswamy, S. Kavitha and R. Nandhakumar, *J. Photochem. Photobiol., A*, 2019, **385**, 112092.

72 R. J. Mumper, J. A. Mcneill and P. Ma, *J. Nanomed. Nanotechnol.*, 2013, **4**, 164.

73 D. B. Hobart, M. A. G. Berg, H. M. Rogers and J. S. Merola, *Molecules*, 2021, **26**, 4331.